Anti-Kasha Fluorescence in Molecular Entities: The Central Role of the Electron-Vibrational Coupling

Koen Veys and Daniel Escudero[*]

Quantum Chemistry and Physical Chemistry Section, Department of Chemistry, KU Leuven,

Celestijnenlaan 200f, 3001 Leuven

CONSPECTUS

According to Kasha's rule, emission of a photon in a molecular system always comes from the lowest excited state. A corollary of this rule, i.e., the Kasha-Vavilov rule, states that the emission spectra are independent of the excitation wavelength. Although these rules apply for most of the molecular systems, violations of these rules are often reported for molecular systems. The prototypical case of a Kasha's rule violation is the fluorescence observed from S_2 in azulene. Thanks to the advances in both theoretical and experimental research, other types of anomalous fluorescence arising from higher-lying excited states (e.g., excitation energy transfer (EET)-based dual emissions, thermally-activated fluorescence etc.), and which mechanistically differ from the azulene-like anomalous fluorescence, are more recurrently reported in the literature. However, the underlying mechanisms leading to these anomalous emissions can be numerous and they are not yet well understood.

In order to shed some light into the above phenomena, this account provides a comprehensive review on this topic. We herein report quantum chemical investigations in target molecular systems breaking Kasha's rule. The latter molecules were chosen as they were unambiguously reported to display anti-Kasha fluorescence. Our studies highlight three different types of anti-Kasha scenarios. Specifically, i) the strong electronic-, weak vibrational-nonadiabatic coupling (NAC) regime (here named as Type I case, i.e., azulene-like); ii) the strong electronic-, strong vibrational-NAC regime (Type II case, i.e., thermally-activated S_2 fluorescence); and the iii) very weak electronic NAC regime (Type III case, i.e., EET dyads). In addition, by combining state-of-the-art quantum chemical calculations with excited-state decay rate theories and appropriate excited-state kinetic models, we provide semi-quantitative estimations of photoluminescence quantum yields for the most rigid molecular entities. Finally, we propose the use of simple theoretical descriptors relying on calculations of the excited-state density difference and the electron-vibrational coupling to classify anomalous emissions according to their coupling scenario.

Besides the fundamental interest of the above investigations, the herein developed computational protocols and descriptors will be useful for the tailored design of dyes with tunable and unconventional fluorescence properties and their exploitation in a wide range of areas, i.e., from organic-light emitting diodes (OLEDs) to bioimaging, small molecule fluorescent probes and photocatalysis. Finally, our theoretical framework enables attaining a holistic understanding of the interconversion processes between excited states, where the electron-vibrational coupling is shown to play a central role in determining the efficacy.

INTRODUCTION

The photochemical properties and the photochemical reactivity of molecules and materials are often governed by their lowest electronically excited states (i.e., the lowest singlet excited state S_1 and/or the lowest triplet excited state T_1). In other words, "polyatomic molecular entities react with appreciable yield only from the lowest excited state of a given multiplicity".[1,2] The latter statement is the formulation of Kasha's rule as given by the IUPAC. Such a rule applies to both photoluminescence processes and photochemical reactions. A corollary of this rule, i.e., the Kasha-Vavilov rule, states that "the quantum yield of luminescence is independent of the wavelength of exciting radiation".[3] However, there are exceptions to both the Kasha's and the Kasha-Vavilov's rules.[4] The first exception was reported for the azulene molecule (see **1a** in **Scheme 1**), which shows anomalous fluorescence from its second singlet excited state (S_2) instead of the more generally observed Kasha-like fluorescence from the lowest singlet excited state (S_1).[5,6] Since then, many other molecular entities have been reported to behave in an anti-Kasha manner. Examples include many derivatives of azulene, Cycl[3.3.3]azine, etc (see **Scheme 1**).[7–11] However, despite the convincing pieces of evidence for Kasha's rule exceptions, there are also other molecular systems that have been dubiously claimed to behave in an anti-Kasha manner. Some of the latter cases have lately been revisited (e.g., diphenyl-octatetraene, diphenyl-tetrazine, etc.) and proven not to strictly break Kasha's rule.[12] Thus, for instance, impurities or other experimental artefacts may lead to the wrong assignment of anti-Kasha events.[12] Anomalous emissions arising from uncorrelated emitters, e.g., from photoproducts or protonated forms, do strictly not violate Kasha's rule.[13] Anomalous emissions arising from the interaction between two correlated emitters in condensed phases (such as e.g., excitation energy transfer between different molecules) can also not be regarded as truly anti-Kasha scenarios.[13] Furthermore, emissions from different excited state

conformers in the lowest adiabatic potential energy surface (PES), such as e.g., the anomalous emission characteristics arising from twisted intramolecular charge transfer (TICT) excited states, are also strictly not anti-Kasha violations.[12]
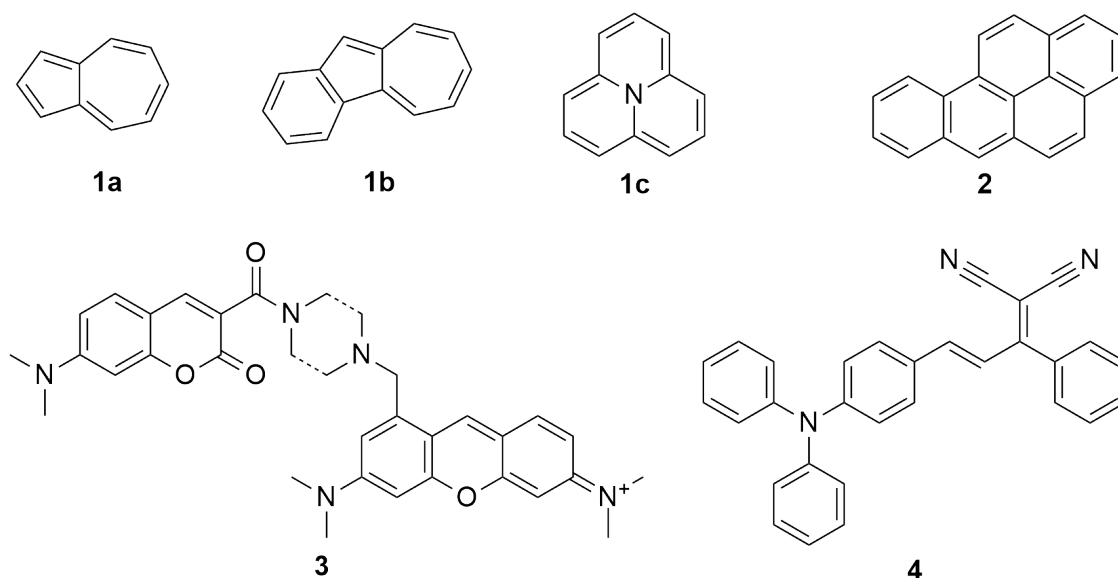
Scheme 1. Molecular structures of all molecules considered in this work.

Photochemistry is kinetically-controlled, and thus, only the fastest processes among all possible photodeactivation channels are observed with an appreciable yield. Upon light excitation the manifold of singlet excited states (S_n) is populated. In Kasha-like scenarios, efficient radiationless deactivation within the singlet manifold follows through vibrational relaxation and internal conversion (IC) processes. These are generally very fast, ultimately leading to the population of the lowest vibrational level of the S_1 state with almost the unity of quantum yield.[14] Because IC processes between the manifold of S_n are generally very fast, other possible decay processes such as e.g., anti-Kasha $S_n \rightarrow S_0$ fluorescence and/or $S_n \rightarrow T_m$ intersystem crossing (ISC) are not competitive to IC[15] (we note that luminescence or anti-Kasha reactivity from a higher-lying excited state than $n,m = 2$ is possible but often less likely possible as n,m increases).[14] This is the ultimate

reason that Kasha's rule applies for most of the molecular entities. For instance, in the specific case of azulene, its anti-Kasha fluorescence originates from the very large energy gap between S_2 and S_1 (i.e., > 1.5 eV). This large energy gap is ultimately responsible for its slowed down $S_2 \rightarrow S_1$ IC process, so that the anti-Kasha $S_2 \rightarrow S_0$ fluorescence becomes kinetically competitive to $S_2 \rightarrow S_1$ IC.[6] These azulene-like behaving compounds are here named as Type I anti-Kasha compounds (see **Scheme 2**). To elaborate a bit more on the dependency of energy gap on the radiative and non-radiative rates, two expressions are useful. Radiative rates (k_r) can be calculated through Einstein's spontaneous emission expression,[16,17]

$$ k_r \approx \frac{\nu^2 \cdot f}{1.5}, \tag{1} $$

while non-radiative rates (k_{nr}) can empirically be described with the energy gap law:[18]

$$ \log(k_{nr}) \approx N - 0.0002 \cdot \nu. \tag{2} $$

Here, ν is the energy gap between the involved states (in cm^{-1}), f the oscillator strength and depending on the transition, N is resp. 12, 10 and 7 for IC, ISC($n,\pi^* \leftarrow \pi,\pi^*$) and ISC ($n,\pi^* \rightarrow n,\pi^*$ or $\pi,\pi^* \rightarrow \pi,\pi^*$). As seen in Eq. (1), k_r depends cubically on the energy gap, while k_{nr} (Eq. (2) decreases exponentially with increasing energy gaps. Eqs. (1-2) do not explicitly incorporate the coupling between the final and initial vibronic states, as included through a Fermi's golden rule (FGR) derived time-independent (i.e., sum-over-states approach) or time-dependent thermal vibration correlation function (TVCF) treatment (see details in the SI).[19,20]

Besides the azulene-like Kasha's rule violation, anti-Kasha S_2 fluorescence might also occur despite a relatively small S_2-S_1 energy gap. This is the case of the anomalous emission observed in e.g., benzopyrene (**2**) (see Type II complexes in **Scheme 2**).[9] This highlights that the actual mechanisms behind anti-Kasha emissions might be of different nature than those for Type I

compounds and that large energy gaps between the involved excited states are not the solely molecular factors determining a given anti-Kasha behavior. Early attempts to classify anti-Kasha anomalous emissions were given by Itoh.[21] More in detail, Itoh differentiates between thermally- and non-thermally-equilibrated scenarios. Among the former scenarios we find for instance the S_2 anomalous emission occurring in e.g., benzopyrene (here named as Type II anti-Kasha compounds). Anti-Kasha emission on Type II compounds occurs due to the combination of two factors: i) the thermal (re)population of S_2 from S_1 at room temperature (i.e., implying energy gaps on the order of kT), and ii) the radiative emission from S_2 is more probable than the one from S_1. However, other anti-Kasha exceptions fall off from Itoh's classification. The anti-Kasha emission observed in **3** occurs neither because of the large S_2-S_1 energy gap (the actual adiabatic energy gap is ca. 0.7 eV), nor because S_2 and S_1 are thermally equilibrated. This highlights that new classifications of anti-Kasha scenarios are needed. In this Accounts, by performing an in-depth quantum chemical investigation of several cases of anti-Kasha exceptions reported in the literature we disclose the central role of the electron-vibrational coupling in determining the different types of anti-Kasha scenarios. This aspect has to date been overlooked in the literature. The degree of electron-vibrational coupling (i.e., weak, strong or intermediate), determines the regime at play. Our approach enables us to unambiguously classify anti-Kasha anomalous emissions with regards to their coupling regime. Thus, as shown later in this Accounts, the S_2 anti-Kasha emission in **3** occurs due to the lack of electron-vibrational coupling between S_2 and S_1, which ultimately leads to a negligible IC process between the involved excited states. In other words, the very weak electronic coupling regime is at play (these compounds belong to the Type III case, see **Scheme 2**). Consequently, in the molecular entities that behave as **3**, the population of S_1 from S_2 can only occur through an intramolecular excitation energy transfer process (i.e., EET). Note that $S_2 \rightarrow S_1$

deactivation mediated by EET is fundamentally different from an $S_2 \rightarrow S_1$ IC process and importantly, it occurs on different timescales. Namely, while IC often takes place in the subpicosecond regime, EET starts to become relevant only at picosecond timescales.[22,23] In Type III compounds, whether anti-Kasha-like emission is observed or not is mainly determined by the efficacy of the $S_2 \rightarrow S_1$ EET process. The subtle competition among all radiative and nonradiative decay processes determines whether a Kasha-like or anti-Kasha-like photochemical scenario will be attained for these systems. In some occasions (like in **3**), a partial $S_2 \rightarrow S_1$ EET process might also occur.[13] The latter scenario may result in dual fluorescence due to the coexistence of both S_2 (anti-Kasha-like) and S_1 (Kasha-like) emissions.
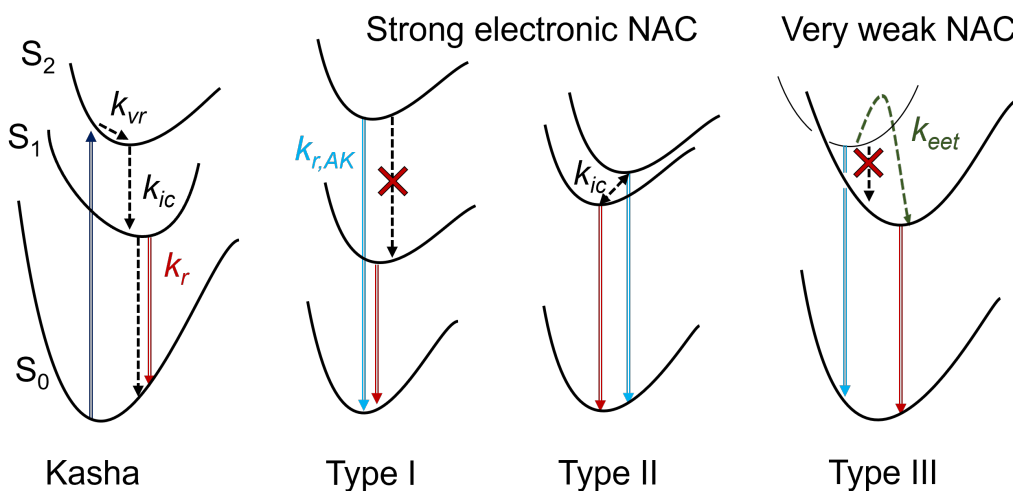
Scheme 2. Schematic representation of Kasha emission (red arrows) and the three different regimes leading to anti-Kasha emission (light blue arrows) after absorption (dark blue) and vibrational relaxation (k_{vr}). For each radiative decay (k_r) there is a competition with internal conversion (k_{ic}) or excitation energy transfer (k_{eet}).

As discussed above, a large variety of kinetics scenarios are possible. From an experimental viewpoint, and regardless of the type of anti-Kasha regime at play, exhaustive steady-state and

time resolved spectroscopic investigations are needed towards an unambiguous assignment of a putative anti-Kasha photochemical scenario.[4] Typical fingerprints of anti-Kasha behavior are excitation wavelength-dependent quantum yields and excitation wavelength-dependent emissive properties. However, a rigorous check of the purity along with recording the photoluminescence excitation spectra and excite state lifetimes with time-resolved experiments are always recommendable. Theoretical research is crucial for the interpretation and rationalization of the complex excited state decay kinetics. For instance, using a combination of state-of-the-art excited state decay rate theories, quantum chemical calculations and excited state kinetics models, we recently developed a computational protocol for the semi-quantitative prediction of anti-Kasha fluorescence in molecules belonging to the strong coupling regime (Type I compounds), which was validated for a series of azulene molecules.[6] In this Accounts, we aim at expanding those previous protocols to cover other coupling regimes (i.e., the very weak electronic NAC regime; Type III) but also to cover thermally-equilibrated scenarios (Type II). Additionally, we propose the use of simple theoretical descriptors relying on calculations of the excited state density difference to classify anomalous emissions according to their coupling scenario. Early attempts by Perfetto *et al.* already include a descriptor of the energy and dipole moment, but neglected the important aspect of the NAC.[24] These tools enable us to make predictions of anti-Kasha fluorescence on a semi-quantitative basis, and more importantly they help us understanding and controlling the energetic and structural parameters determining anomalous fluorescence. By predicting and controlling complex and unusual photochemistry we might lead to the next breakthrough in light-to-energy conversions: from organic-light emitting diodes (OLEDs) to organic lasers, organic solar cells, bioimaging and photocatalysis, which are applications where anti-Kasha photochemistry have great prospects to contribute to.

THEORETICAL AND COMPUTATIONAL FRAMEWORK

Photoluminescence quantum yields (PQYs) are determined as the ratio of the radiative rate over the sum of all possible decay rates. Calculating PQYs from first principles implies the need to accurately calculate both radiative and all non-radiative rates. For the excited-state decay rate calculations, quantum chemistry calculations should be coupled to the calculations of electron-vibrational couplings (EVC) and the vibrational analysis.[25] Thus, the calculation of vibronically-resolved absorption and emission spectra, radiative rates, internal conversion (IC) rate, and intersystem crossing, etc. is nowadays feasible for molecular entities.[25,26] In practical terms, one needs to i) optimize the geometry in all relevant electronic states where transitions are considered and to ii) compute first and second derivatives at these geometries. In addition, for the EVC part and for the evaluation of the Franck-Condon (FC) integrals, we make use of a multidimensional harmonic oscillator model where displacements, distortions and Duschinsky rotations of the potential energy surfaces are taken into account. Both for spectra and rate calculations, the thermal vibration correlation function (TVCF) and path integral methods are used to deal with the complex multidimensional integrals (time dependent approach), and thus avoiding the tedious summation over a tremendous amount of vibrational states (time independent approach). This theory has extensively been reviewed elsewhere,[19,20,27] so only some key elements are mentioned in the following, while the full theoretical framework is summarized in the supporting information, along with the complete computational details. In general, the rate, k_{if}, between two states (i, f) is given by Fermi's Golden Rule (FGR) expression:

$$k_{if} = \frac{2\pi}{\hbar} \left| \langle \Psi_f | H' | \Psi_i \rangle \right|^2 \rho, \tag{3}$$

where Ψ is the total wavefunction, H' the perturbation operator and ρ the density of final states. Starting from the FGR expression, one can derive different rates, depending on the chosen perturbation.[15] Using the transition dipole moment as a perturbation, expressions for k_r can be derived. If the non-adiabatic coupling (NAC) operator is used as a perturbation instead, the IC rate follows. Analogously, rates for other physical processes (i.e., for EET, ISC) can be derived as well. It is interesting to note that by applying the Condon approximation for the IC rate, the NAC can be divided into an electronic and vibrational part,[19,20] which will help us to distinguish between the different anti-Kasha types.

The electronic part of the NAC can already provide important hints into the actual mechanism of decay between excited states. Here we derive a density-based descriptor, enabling to both visualize and quantify the electronic part of the NAC (see details in the SI).

RESULTS

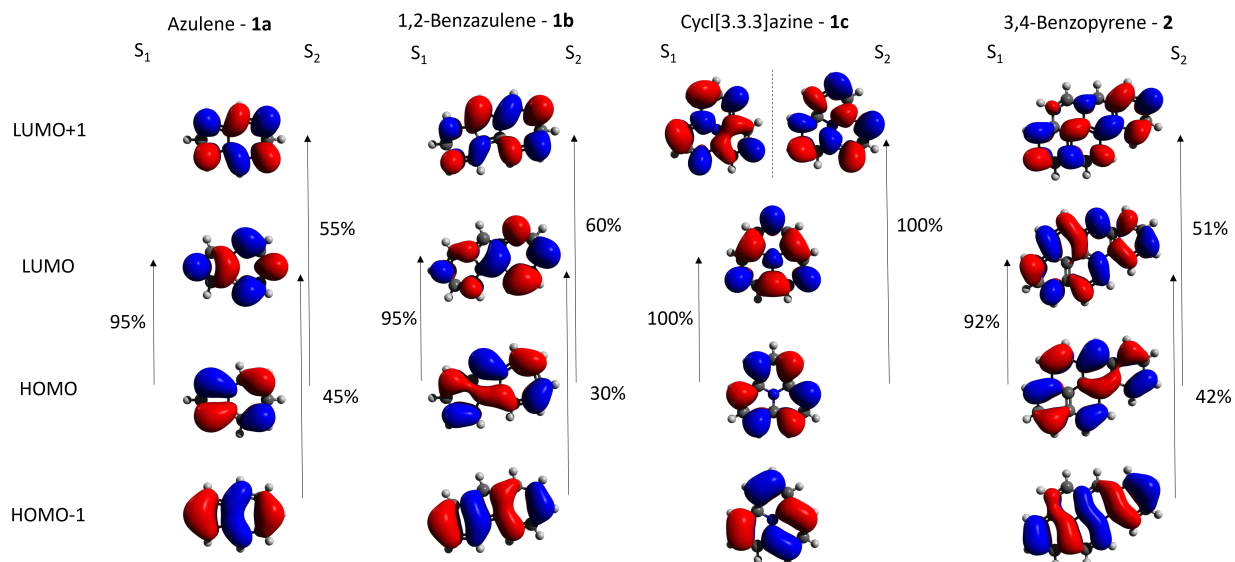**Type I: Strong Electronic, Weak Vibrational NAC**

Figure 1. Kohn-Sham frontier molecular orbitals of **1a-c** and **2** with the corresponding weights of the electronic transitions contributing to S_1 and S_2. (TD-CAM-B3LYP/6-31+G(d))
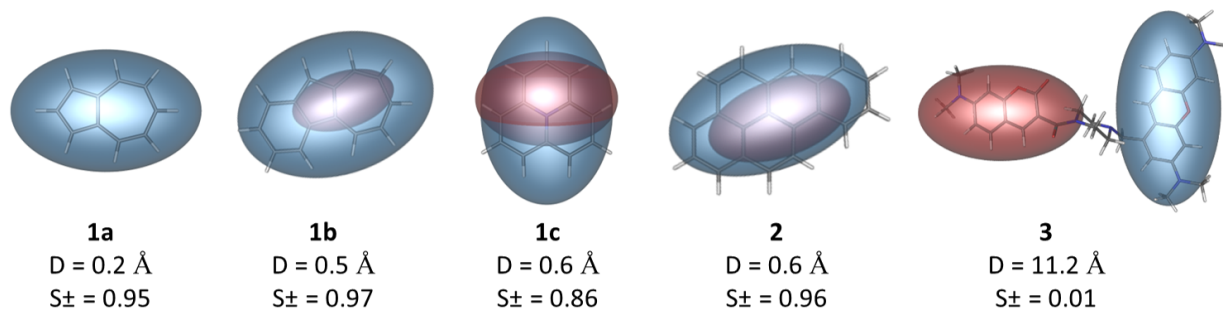

Figure 2. Density-based visualization of the C_+ and C_- descriptors along with the numerical values of the D and S± indexes for **1a-c**, **2** and **3**. For **1a**, the S_1 (red) zone disappears at this isovalue (0.00015).

The first type of anti-Kasha regime is marked by a large energy difference between S_2 and S_1, resulting in a slow IC process, making it able to compete with fluorescence from S_2. This is indeed what we see when looking at the calculated energies for **1a-c** (**Table 1**), where for all the molecules, the computed adiabatic energy difference between S_1 and S_2 exceeds 1.5 eV. Looking

at the orbitals involved in these transitions (**Figure 1**), one can see that for **1a**, **1b** (and other azulene derivatives as in ref. [6]) the frontier orbitals are rather similar. The S_1 is a HOMO → LUMO transition, with the orbitals located on different atoms, whereas the S_2 is a HOMO-1 → LUMO & HOMO → LUMO+1 transition (see the weights of each electronic transition in **Figure 1**). Conversely, the excited states of **1c** differ from those of **1a-b** because its S_2 state is a 100% HOMO → LUMO+1 transition and it is almost degenerate with the S_3 state, which corresponds to a HOMO → LUMO+2 transition. Because of this symmetry-driven degeneracy, both S_2 and S_3 states have similar properties and rates, so only one state is considered herein for simplicity.

Density-based descriptors were calculated for the S_2-S_1 interconversion for compounds **1a-c**. For details about the indexes, see SI. The numerical results along with the visual representation of the different descriptors can be seen in **Figure 2**. **1a-c** possess a small D-index (between 0.2 - 0.6 Å), and an S± index close to 1. Consequently, these values correspond to a strongly electronically coupled situation for the S_2-S_1 interconversion of Type I systems. Visually, this is reflected by two fully overlapping S_1 and S_2 lobes. For **1a-c**, the S_1 density is less similar to the ground state than the S_2 density, which leads to a smaller S_1 (red) lobe. All the above computed facts highlight that for Type I compounds the S_2 to S_1 interconversion is electronically allowed (and thus, the main interconversion process is a direct IC process), although slowed down because of the large S_2-S_1 energetic difference, which results in small overlap between vibrational wavefunctions (i.e., weak vibrational NAC regime).

Table 1. Calculated (ADC(2)/def2-TZVP) vertical energy differences (E_v, eV), adiabatic energy differences (E_{ad}, eV), and oscillator strengths (f) for the S_1 and S_2 states of **1a-c**.

$E_v(S_0 \rightarrow S_1)$	$E_v(S_0 \rightarrow S_2)$	$E_v(S_1 \rightarrow S_0)$	$E_v(S_2 \rightarrow S_0)$	$E_{ad}(S_0\text{-}S_1)$	$E_{ad}(S_0\text{-}S_2)$	$f(S_1)$	$f(S_2)$

1a	2.24	3.85	1.48	3.70	1.86	3.77	0.003	0.007
1b	2.35	3.56	1.27	3.18	1.53	3.22	0.005	0.075
1c	1.00	3.01	0.88	2.69	0.94	2.89	0.000	0.219

Table 2. Calculated radiative (k_r, s^{-1}) and internal conversion rates (k_{ic}, s^{-1}), as well as Photoluminescence Quantum yields (PQY, unity) for the different states of **1a-c**.

	$S_1 \rightarrow S_0$		$S_2 \rightarrow S_0$	$S_2 \rightarrow S_1$		PQY(S_1)	PQY(S_2)
	k_r	k_{ic}	k_r	k_r	k_{ic}		
1a	4E+05	1E+10	2E+07	1E+05	1E+09	3E-05	2E-02
1b	4E+05	8E+11	7E+07	3E+04	4E+10	5E-07	2E-03
1c	9E+03	1E+12	8E+07	9E+06	8E+10	9E-09	9E-04

Now, let us analyze the results of the computed rates and the PQYs for Type I compounds. The results are listed in **Table 2**. For **1a-c**, the PQY from S_1 is rather low, due to the small S_1-S_0 adiabatic energy difference, resulting in a high IC rate (10^{10} – 10^{12} s^{-1}) and a low fluorescence rate (10^3 – 10^5 s^{-1}). On the contrary, the S_2-S_0 gap is much larger, resulting in a generally higher k_r value from S_2 (10^6 – 10^8 s^{-1}). Because of the large S_2-S_0 gap, IC from S_2 to S_0 will be negligible as compared to the main IC decay, i.e., S_2-S_1, and thus making it unnecessary to calculate these rates for which the harmonic approximation is also doubtful. Overall, this results in a non-negligible PQY value from S_2, which is a few orders of magnitude larger than the PQY from S_1; in accordance with the experimental observations of anti-Kasha emission for **1a-c**.

Type II: Strong Electronic, Strong Vibrational NAC

In contrast to the previous type, where a large energy difference is causing slow IC to S_1, a very small energy difference between S_2 and S_1 leads to the strong electronic and strong nuclear coupling regime. This gives the possibility of a thermal equilibrium between the two excited states, resulting in the possible (re)population of S_2 from S_1. To be able to use the harmonic approximation for the (forward and back) internal conversion here, the PES of S_1 and S_2 need to be nested, since otherwise an Arrhenius-type expression needs to be used for the interconversion between the excited states.[30,31] As a representative example of Type II compounds, we explore the excited states of [3,4]-benzopyrene (**2**), which experimentally displays dual fluorescence.[9] In benzopyrenes, but also in naphthalene and other acenes, the first two excited states typically correspond to the bright La state (a HOMO → LUMO transition) and the dark Lb state (HOMO → LUMO+1 & HOMO-1 → LUMO transitions).[32] When these two states are close in energy, it is often difficult to predict their correct ordering, and high-level ab initio quantum chemical calculations are often needed to get the correct adiabatic energy gap.[32] This is exactly what we see when calculating the La and Lb states of **2** with TD-CAM-B3LYP (for the exact composition of the La and Lb states see **Figure 1**). Thus, as shown in **Table 3**, the La and Lb states are swapped as compared to the experimental values. It is only when doing single point STEOM-DLPNO-CCSD calculations, that the states are ordered correctly.

Both Type I and Type II anti-Kasha compounds have a strong electronic coupling between the S_1 and S_2 states, resulting in a similar density-based descriptor. This is shown in **Figure 2**, where the calculated values and visual image for the descriptors of **2** correspond well to those calculated for **1a-c**. The difference in the two types thus only comes from the difference in the amount of vibrational coupling, related to the energy difference between the involved excited states.

Table 3. Calculated vertical energy differences (E_v, eV), adiabatic energy differences (E_{ad}, eV) and oscillator strengths (f) for the La and Lb states of **2** at different levels of theory. (STEOM-DLPNO-CCSD single point calculations at the TD-CAM-B3LYP/6-31+G(d) geometry). Experimental adiabatic energies are also given as a reference.[9]

		$E_v(S_0{\rightarrow}L_x)$	$E_v(L_x{\rightarrow}S_0)$	$E_{ad}(S_0 - L_x)$	$f(L_x)$
TD-CAM-B3LYP /6-31+G(d)	La	3.55	3.10	3.32	0.402
	Lb	3.76	3.50	3.63	0.019
STEOM-DLPNO-CCSD/aug-CC-pVTZ	Lb	3.20	2.98	2.83	0.002
	La	3.65	3.24	3.12	0.473
Experimental	Lb			3.08	
	La			3.24	

For the calculation of the actual PQYs for S_1 and S_2 of **2**, all the radiative, IC and ISC rates need to be concomitantly evaluated, whereafter a coupled system of differential equations is solved in order to deal with the thermal equilibrium between the two states. However, because here we only aim at a semi-quantitative estimation of the PQYs, the experimental PQY ratio, i.e., PQY(La)/PQY(Lb), can be used to compare theory and experiments. Experimentally, this ratio varies between 0.015 and 0.18, depending on solvent and temperature.[9,33,34] This means that the lower-lying state, which corresponds to the Lb state is populated in a significantly larger extent than the bright La state. Because the interconversion between La and Lb is much faster than all other possible competing deactivation decays, an equilibrium is reached, and the PQY ratio will depend neither on the IC rates to other states, nor on possible ISC processes populating triplet

excited states. Therefore, the PQY ratio can be safely approximated as k_{ic}(Lb→La)/k_{ic}(La→Lb)*k_r(La→S$_0$)/k_r(Lb→S$_0$).[35] For the accurate calculation of IC rates, having a correct adiabatic energy gap is especially important. Note that the IC rate values decrease very fast when the gap becomes more negative, i.e. at the uphill part of the log(IC)-vs-Ead-parabola (see **Figure S1**). Instead, at the top of this parabola (i.e., with small, positive energy differences, see in **Figure S1**), the rate is less dependent on the energy gap. This is illustrated with the data presented in **Table 4**, where the effect of the calculated adiabatic energy gaps with different levels of theory on the computed IC rates is shown. On the contrary, this is less of a problem for the radiative rates, because the large La/b-S$_0$ gaps and the oscillator strengths remaining relatively similar at the different levels of theory. As shown in **Table 4**, the bright La state has a radiative rate which is about one order of magnitude larger than the one for the dark Lb state (10^8 vs 10^7 s^{-1}). At the TD-CAM-B3LYP level of theory, the PQY ratio is extremely overestimated because of the wrong state ordering at this level. It is only when using an accurate adiabatic energy gap from the STEOM-DLPNO-CCSD calculations, that the PQY ratio starts to get in agreement with the experimental one. The adiabatic gap however, is still ca. 0.15 eV overestimated at the STEOM-DLPNO-CCSD level as compared with the experiment. Obtaining more accurate adiabatic gaps beyond the STEOM-DLPNO-CCSD level is beyond the scope of this work, and thus, we also used the experimental gap in the rate calculations. The latter approach yielded a PQY ratio of ~1 (see **Table 4**), which is within the same order of magnitude as the experimental ratio. The remaining error probably comes from using non-adiabatic couplings which are still calculated at the TD-CAM-B3LYP level, and thus, inferring that the above procedure can provide accurate results, only in the case that a very accurate energy differences and couplings are provided.

Table 4. Calculated radiative (k_r, s^{-1}) internal conversion rates (k_{ic}, s^{-1}) between the La and Lb states of **2**, using different levels of theory for the adiabatic energy difference (ΔE_{ad}, eV), all based on TD-CAM-B3LYP/6-31+G(d) geometries and frequencies. The ratio k_{ic}(Lb→La)/k_{ic}(La→Lb) *k_r(La→S$_0$)/k_r(Lb→S$_0$) is given as well.

	TD-CAM-B3LYP/ 6-31+G(d)	STEOM-DLPNO-CCSD/aug-CC-pVTZ	Exp. ΔE_{ad}
ΔE_{ad}	-0.30	0.29	0.15
k_r(La → S$_0$)	1E+08	1E+08	1E+08
k_r(Lb → S$_0$)	2E+07	7E+06	9E+06
k_{ic}(La → Lb)	5E+07	2E+13	3E+13
k_{ic}(Lb → La)	2E+14	1E+10	2E+12
ratio (exp = 0.015-0.18)	5E+07	0.008	1

Type III: Very Weak Electronic NAC

The last type of anti-Kasha regime is neither characterized by a very large energy difference between S$_2$ and S$_1$ (Type I compounds), nor by S$_2$ and S$_1$ being thermally equilibrated (Type II compounds). Conversely, in Type III compounds, S$_2$ and S$_1$ are instead separated through space, which leads to a complete lack of electron-vibrational coupling between the two excited states. Besides the above basic requirements, additional prerequisites are mandatory to attain substantial S$_2$ emission in Type III compounds. For instance, the radiative process from S$_2$ should outcompete to the EET process from S$_2$ to S$_1$, but also to the IC from S$_2$ to S$_0$. If the EET process and the radiative decay rate from S$_2$ fall within the same order of magnitude this often results into dual fluorescence scenarios (provided that the radiative rate from S$_1$ outcompetes to the IC from S$_1$ to

S_0). Intramolecular Forster Resonance Energy Transfer (FRET) dyads are the most likely molecular systems that may fall within Type III compounds. As a model representative system of a Type III compound, we took a coumarin-pyronine FRET-based dyad, **3**, which was recently investigated by Kawagoe et al.[10] Experimentally, they measured dual fluorescence at 479 nm and 584 nm, with a PQY ratio of $PQY_{479}/PQY_{584} = 0.5$. In **Figure 2**, the numerical results along with the visual representation of the different density-based descriptors are shown for the S_2-S_1 interconversion of **3**. A large D-index (11.2 Å) and an S± index close to zero highlight the very weakly electronically coupled situation, which applies for Type III compounds. Visually, this is reflected by two non-overlapping S_1 and S_2 lobes. Similarly, the orbital transitions are spatially separated as well, as can be seen in **Figure S4**. The use of the standard formulas to calculate an IC process between excited states is no longer valid here, and thus, an EET rate between S_2 and S_1 was calculated instead (see computational details in the SI).

In Table 5 the computed energies, oscillator strengths and rates are listed for **3**. TD-CAM-B3LYP calculations show that both S_1 and S_2 are very bright states (f > 1). S_1 and S_2 are respectively located on the pyronine and the coumarin moieties. The calculated emission energies peak at 395 and 488 nm. The latter values are ca. 0.5 eV higher than their experimental counterparts, which can be inferred, among other possible sources of errors, to the limitations of the linear response polarizable continuum solvent model to model emission processes. In particular, the experimental aqueous buffer is represented in this work by a dielectric solvent cage, which lacks specific solvent-solute interactions. However, the investigation with more advanced solvation models goes beyond the scope of this study and semi-quantitative results can still be obtained with the approach used here, as the errors for S_1 and S_2 are systematic.

We now turn the discussion into the calculated rates of **3**. We note that attaining reliable rate calculations in large, flexible molecules (such as e.g., **3**), where the harmonic approximation is likely to fail, is rather difficult. Here we use a fragment-based approach to calculate the IC and radiative rates of the dyad, i.e., the latter rate calculations are performed at the isolated fragments of the dyad. The fragments are smaller and more rigid than the dyad and thus, it is more likely that the harmonic approximation will hold true. We note that this is a valid approach for **3** because of the lack of electron-vibrational coupling between S_2 and S_1 (see below). Thus, the ground and first excited states of the pyronine and coumarin moieties, were optimized separately. The absorption, emission and adiabatic energies deviate by less than 0.01 eV from the S_1 and S_2 state of **3**, proving the validity of our approach. Conversely, to calculate the EET rate calculation the optimized geometry of the full dyad was used instead. Looking then at the rate calculations and subsequent PQYs (Table 5**b**), one can see that the main deactivation mechanism of S_2 is through an EET to S_1, which is much faster than the IC to the ground state (compare $\sim 10^{11}$ vs $\sim 10^7$ in Table 5**b**). The EET coupling was calculated to be 0.005 eV (41 cm^{-1}). It originates from the large transition dipole moments of S_2 and S_1, but the almost perpendicular orientation between them leads to less sizable coupling (see **Figure S3**). For the sake of clarity, the PQYs for S_1 and S_2 are respectively calculated using:

$$\Phi_{S_1} = \frac{k_{r,pyr,10}}{k_{r,pyr,10} + k_{ic,pyr,10}} \; and \; \Phi_{S_2} = \frac{k_{r,cou,10}}{k_{r,cou,10} + k_{ic,cou,10} + k_{eet,21}}. \qquad (4)$$

Using all the calculated rates we obtain a PQY(S_2)/PQY(S_1) ratio of 0.3 (see the computed PQYs values in **Table 5b**). Furthermore, by using the experimental energies within the rate calculations, this ratio becomes 0.7 (see **Table S2**). This is in excellent agreement with the experimental ratio of ca. 0.5. All in all, the density-based descriptors for the S_2-S_1 interconversion of **3** highlight a

different anti-Kasha scenario for Type III compounds, as compared to those for Type I and Type II compounds. As demonstrated here for **3**, not only this can be predicted qualitatively by inspecting the density indexes, but also semi-quantitative estimations of the PQYs of Type III compounds are attainable. We also note that for Type III compounds the energy gap is less of an issue than for Type I-II compounds. Specifically, as long as there is some spectral overlap between the emission and absorption spectrum of S_2 and S_1, respectively; the corresponding EET process can take place. This means that a gap of 0.7 eV (as for **3**) is acceptable but a negligible energy gap would be acceptable too.

Table 5. a) Calculated vertical energy differences (E_v, eV), adiabatic energy differences (E_{ad}, eV), oscillator strengths (f) and EET coupling (eV) for the S_1 and S_2 states of 3 (TD-CAM-B3LYP/6-31+G(d)). b) Calculated radiative (k_r, s^{-1}), internal conversion (k_{ic}, s^{-1}) and excitation energy transfer rates (k_{eet}, s^{-1}). 3_{pyr} and 3_{cou} are respectively the optimized pyronine and coumarin fragments.

a)	$E_v(S_0 \rightarrow S_x)$	$E_v(S_x \rightarrow S_0)$	E_{ad}	f	EET Coupling
3 - S_1	2.86	2.54 (2.12)	2.59	1.396	0.0051
3 - S_2	3.65	3.14 (2.59)	3.29	1.074	

b)	k_r	k_{ic}/k_{eet}	PQY
3_{pyr} - $S_1 \rightarrow S_0$	3E+08	2E+10	0.014
3_{cou} - $S_1 \rightarrow S_0$	3E+08	1E+07	0.004
3 - EET - $S_{2,cou} \rightarrow S_{1,pyr}$		8E+10	

20

Alternative anti-Kasha scenarios: Intermediate Coupling regime

Compounds **1**-**3** have been successfully classified into different anti-Kasha cases according to the electron-vibrational coupling regime at play. However, there might be other compounds falling out from the above classification. Here, we revisit the excited state characteristics of compound **4** (a dicyano-vinyl derivative, see **Scheme 1**). Recently, two groups[36,37] independently reported Kasha-like emission for this molecule, while Gong *et al.*[11] measured anti-Kasha emission in acetonitrile by exciting at 380 nm. A theoretical investigation of **4** reveals that there is neither a small nor a large energy separation between S_1 and S_2, while the excited states are also not completely separated in space (see below). Note that this situation is likely found for through-bond energy transfer based (TBET) dyads as well, although to our knowledge anomalous emissions have not yet been reported for any TBET dyad.

Table 6. Calculated vertical energy differences (E_v, eV), adiabatic energy differences (E_{ad}, eV) and oscillator strengths (f), along with the associated orbital transitions for the S_1 and S_2 states of **4**. (TD-CAM-B3LYP/6-31+G(d).) Dihedral angle φ at the different minima is reported.

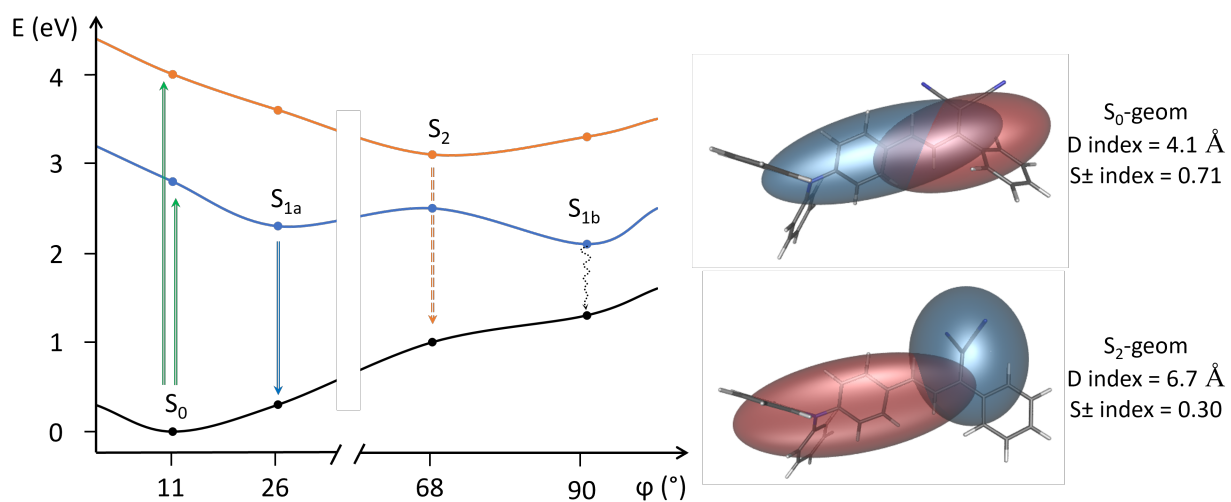|	$E_v(S_0{\rightarrow}S_x)$	$E_v(S_x{\rightarrow}S_0)$	f	orbital transitions	φ (°)
S_{1a}	2.81	2.05	1.52	91% HOMO→LUMO	26
S_{1b}		0.78	0.00	97% HOMO→LUMO	68
S_2	4.00	2.10	1.36	58% HOMO-1→LUMO 30% HOMO→LUMO	90
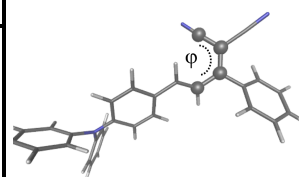
Figure 3. Left: PES representation of the S_1 and S_2 states of **4**, as a function of the dihedral angle φ (see its definition in **Table 6** and the energies in **Table S3**). Right: Density-based descriptor of **4**, at the minimal geometry of S_0 and S_2.

We explored the potential energy surfaces of the S_1 and S_2 with TD-CAM-B3LYP calculations. (**Figure 3** shows schematically relevant stationary points in the S_1 and S_2 PES.) Specifically, there are two minima in the S_1 surface: S_{1a} and S_{1b}. S_{1a} lays geometrically close to the ground state and has an oscillator strength of 1.5, due to the large overlap between HOMO and LUMO (**Figure S5**). Relaxation along the S_{1a} PES leads to another local minimum (S_{1b}) which is adiabatically 0.2 eV lower in energy. The relaxation mainly involves the twisting of the dihedral angle of the dicyano group, which in S_{1b} displays a perpendicular configuration with respect to the vinyl group (compare the values for the dihedral angle φ in Table 6). Geometrical relaxation to S_{1b} is coupled to significant orbital relaxation, as it can be seen in **Figure S5**. Specifically, and as compared to the Franck-Condon situation, the HOMO becomes more localized on the vinyl part, while the LUMO localizes in the other part of the molecule, resulting in the S_{1b} becoming a dark state (f=0, see **Table**

6). S_{1b} is thus of significant TICT character. Conversely, relaxation on the S_2 potential energy surface leads to the S_2 minimum, which geometrically lays in between S_{1a} and S_{1b}. The S_2 state is mainly characterized by a HOMO-1 → LUMO electronic transition (see **Table 6**), leading to a higher orbital overlap, a higher oscillator strength and thus, a possible emissive state. However, at the S_2 minimum, the vertical energy difference between S_2 and S_1 is only 0.6 eV at the TD-CAM-B3LYP level, which is typically not enough to have an azulene-like anti-Kasha emission. At the same time, looking at the density descriptor in **Figure 3**, a D and S± index of resp. 6.7 Å and 0.3 is found at the S_2 minimum. Therefore, the two states do not fully overlap, but they are not totally separated in space either, and thus, guaranteeing at least some electron-vibrational coupling between S_2 and S_1. Under these circumstances it seems unlikely that an EET process is fast enough to compete with a standard IC mechanism. However, due to the overlap of the states and the large geometrical changes between states (including rotations), the harmonic approximation will likely not be valid, making it unfeasible to perform accurate IC calculations for **4**. Therefore, even though the combination of an intermediate energy difference and some electronic separation could result in anti-Kasha emission, further (time resolved) spectroscopic evidence is needed to put the putative anti-Kasha emission observed for **4** on firmer grounds. Also high level quantum chemical calculations could give some more insight here, because single point ADC(2) calculations already result in a slightly different PES representation, as it is discussed in the supporting information (**Table S3** and **Figure S6**). In this regard, contradictory results have been experimentally observed, so that one cannot fully disregard an experimental artifact either; and thus prevent us to extract further conclusions. Note also that our current theoretical machinery to calculate rates and PQYs is a static approach. Explicitly considering the excited state dynamics and the specific solvent-solute interactions might be important in the theoretical framework, in order to address anomalous

emissions on semi-rigid molecules, such as e.g., compound **4** as well as in other TICT-like compounds.

CONCLUSIONS&OUTLOOK

In this Accounts, quantum chemical investigations have been performed in target molecular systems breaking Kasha's rule. The in-depth analysis of the different cases enables us to disclose different mechanistic regimes leading to anomalous emissions in molecular entities. The electron-vibrational coupling plays a central role in determining the given regime. Our studies highlight three different types of anti-Kasha scenarios, namely: i) the strong electronic-, weak vibrational-NAC regime (Type I); ii) the strong electronic-, strong vibrational-NAC regime (Type II); and the iii) very weak electronic NAC regime (Type III case). Anomalous emissions on molecules belonging to intermediate coupling regimes may also be possible, but a definitive confirmation of the latter regimes needs further experimental and theoretical support. Additionally, we have developed simple and cheap theoretical descriptors to unambiguously classify anomalous emissions according to their regime at play. We also demonstrate that semi-quantitative estimations of PQYs in good agreement with the experimental evidence are possible for the herein investigated compounds, regardless of their regime at play. We note that the latter PQYs calculations are only of sufficient accuracy for rigid molecular entities, for which the harmonic approximation holds true. Importantly, our protocols are based on a static approach examining computed ingredients at minima structures on the corresponding PES. However, dynamical effects might also be important in modulating the presence/absence of anomalous emissions. All in all, this Accounts is not only of fundamental relevance, as it contributes to our understanding of the interconversion processes between excited states, but it will also be useful for the design of tailored dyes displaying unconventional fluorescence properties.

ASSOCIATED CONTENT

Supporting Information

The supporting information contains the following data: extra theoretical and computational details, $\log(k_{ic})$-vs-E_{ad}-plot of **2**, structures of **3**$_{pyr}$ and **3**$_{cou}$, TDM visualization of **3**, radiative and non-radiative rates using the experimental E_{ad} of **3**, frontier molecular orbital plots of **3** and **4**, adiabatic energies of **4**, example input files and xyz-coordinates of the optimized geometries.

AUTHOR INFORMATION

Corresponding Author

*Daniel Escudero. E-mail: Daniel.escudero@kuleuven.be

Author Contributions

K. V.: Investigation, Formal analysis, Writing - review & editing. D. E.: Conceptualization, Formal analysis, Writing - review & editing, Funding acquisition. All authors have given approval to the final version of the manuscript.

REFERENCES

(1)   Braslavsky, S. E. Glossary of Terms Used in Photochemistry, 3rd Edition (IUPAC Recommendations 2006). *Pure Appl. Chem.* **2007**, *79* (3), 293–465. https://doi.org/10.1351/pac200779030293.

(2)   Kasha, M. Characterization of Electronic Transitions in Complex Molecules. *Discuss. Faraday Soc.* **1950**, *9* (c), 14. https://doi.org/10.1039/df9500900014.

(3)   *The IUPAC Compendium of Chemical Terminology*; Gold, V., Ed.; International Union of Pure and Applied Chemistry (IUPAC): Research Triangle Park, NC, 2019. https://doi.org/10.1351/goldbook.

(4)   Demchenko, A. P.; Tomin, V. I.; Chou, P.-T. Breaking the Kasha Rule for More Efficient Photochemistry. *Chem. Rev.* **2017**, *117* (21), 13353–13381. https://doi.org/10.1021/acs.chemrev.7b00110.

(5)   Viswanath, G.; Kasha, M. Confirmation of the Anomalous Fluorescence of Azulene. *J. Chem. Phys.* **1956**, *24* (3), 574–577. https://doi.org/10.1063/1.1742548.

(6)   Veys, K.; Escudero, D. Computational Protocol To Predict Anti-Kasha Emissions: The Case of Azulene Derivatives. *J. Phys. Chem. A* **2020**, *124* (36), 7228–7237. https://doi.org/10.1021/acs.jpca.0c05205.

(7)   Awuku, S.; Bradley, S. J.; Ghiggino, K. P.; Steer, R. P.; Stevens, A. L.; White, J. M.; Yeow, C. Photophysics and Spectroscopy of 1,2-Benzazulene. *Chem. Phys. Lett.* **2021**, *784*, 139114. https://doi.org/10.1016/j.cplett.2021.139114.

(8)   Leupin, W.; Wirz, J. Low-Lying Electronically Excited States of Cycl[3.3.3]Azine, a

Bridged 12.Pi.-Perimeter. *J. Am. Chem. Soc.* **1980**, *102* (19), 6068–6075. https://doi.org/10.1021/ja00539a016.

(9)   Hoytink, G. J. On the "Anomalous" Flourescence of 3,4-Benzypyrene in the Vapour Phase. *Chem. Phys. Lett.* **1974**, *26* (1), 16–19. https://doi.org/10.1016/0009-2614(74)89073-1.

(10)   Kawagoe, R.; Takashima, I.; Uchinomiya, S.; Ojida, A. Reversible Ratiometric Detection of Highly Reactive Hydropersulfides Using a FRET-Based Dual Emission Fluorescent Probe. *Chem. Sci.* **2017**, *8* (2), 1134–1140. https://doi.org/10.1039/C6SC03856E.

(11)   Gong, J.; Wei, P.; Liu, J.; Chen, Y.; zhao, zheng; Zhao, W.; Ma, C.; Lam, J.; Wong, K. S.; Li, Y.; et al. Anti-Kasha System by Design: A New Gateway for Cell Differentiation Through Machine Learning. *ChemRxiv* **2020**. https://doi.org/10.26434/chemrxiv.12355940.

(12)   del Valle, J. C.; Catalán, J. Kasha's Rule: A Reappraisal. *Phys. Chem. Chem. Phys.* **2019**, *21* (19), 10061–10069. https://doi.org/10.1039/C9CP00739C.

(13)   Gierschner, J.; Behera, S. K.; Park, S. Y. Dual Emission: Classes, Mechanisms and Conditions. *Angew. Chemie Int. Ed.* **2020**, anie.202009789. https://doi.org/10.1002/anie.202009789.

(14)   Laboe, M.; Lahiri, J.; Mohan T. M., N.; Liang, F.; Levine, B. G.; Beck, W. F.; Dantus, M. Linear and Nonlinear Optical Processes Controlling S 2 and S 1 Dual Fluorescence in Cyanine Dyes. *J. Phys. Chem. A* **2021**, *125* (45), 9770–9784. https://doi.org/10.1021/acs.jpca.1c05772.

(15)   Köhler, A.; Bässler, H. *Electronic Processes in Organic Semiconductors*; Wiley-VCH Verlag GmbH & Co. KGaA: Weinheim, Germany, 2015.

https://doi.org/10.1002/9783527685172.

(16) Shuai, Z. Thermal Vibration Correlation Function Formalism for Molecular Excited State Decay Rates. *Chinese J. Chem*. **2020**, *38* (11), 1223–1232. https://doi.org/10.1002/cjoc.202000226.

(17) Zeng, W.; Gong, S.; Zhong, C.; Yang, C. Prediction of Oscillator Strength and Transition Dipole Moments with the Nuclear Ensemble Approach for Thermally Activated Delayed Fluorescence Emitters. *J. Phys. Chem. C* **2019**, *123* (15), 10081–10086. https://doi.org/10.1021/acs.jpcc.9b02376.

(18) Kln, P.; Wirz, J. A Crash Course in Photophysics and a Classification of Primary Photoreactions. In *Photochemistry of Organic Compounds*; John Wiley & Sons, Ltd: Chichester, UK, 2009; pp 25–72. https://doi.org/10.1002/9781444300017.ch2.

(19) Niu, Y.; Peng, Q.; Deng, C.; Gao, X.; Shuai, Z. Theory of Excited State Decays and Optical Spectra: Application to Polyatomic Molecules. *J. Phys. Chem. A* **2010**, *114* (30), 7817–7831. https://doi.org/10.1021/jp101568f.

(20) Humeniuk, A.; Bužančić, M.; Hoche, J.; Cerezo, J.; Mitrić, R.; Santoro, F.; Bonačić-Koutecký, V. Predicting Fluorescence Quantum Yields for Molecules in Solution: A Critical Assessment of the Harmonic Approximation and the Choice of the Lineshape Function. *J. Chem. Phys.* **2020**, *152* (5), 054107. https://doi.org/10.1063/1.5143212.

(21) Itoh, T. Fluorescence and Phosphorescence from Higher Excited States of Organic Molecules. *Chem. Rev.* **2012**, *112* (8), 4541–4568. https://doi.org/10.1021/cr200166m.

(22) Cupellini, L.; Corbella, M.; Mennucci, B.; Curutchet, C. Electronic Energy Transfer in

Biomacromolecules. *WIREs Comput. Mol. Sci.* **2019**, *9* (2). https://doi.org/10.1002/wcms.1392.

(23)   Azarias, C.; Cupellini, L.; Belhboub, A.; Mennucci, B.; Jacquemin, D. Modelling Excitation Energy Transfer in Covalently Linked Molecular Dyads Containing a BODIPY Unit and a Macrocycle. *Phys. Chem. Chem. Phys.* **2018**, *20* (3), 1993–2008. https://doi.org/10.1039/C7CP06814J.

(24)   Perfetto, A.; Maschietto, F.; Ciofini, I. Following Excited States in Molecular Systems Using Density-Based Indexes: A Dual Emissive System as a Test Case. *J. Photochem. Photobiol. A Chem.* **2019**, *383*, 111978. https://doi.org/10.1016/j.jphotochem.2019.111978.

(25)   Niu, Y.; Li, W.; Peng, Q.; Geng, H.; Yi, Y.; Wang, L.; Nan, G.; Wang, D.; Shuai, Z. MOlecular MAterials Property Prediction Package (MOMAP) 1.0: A Software Package for Predicting the Luminescent Properties and Mobility of Organic Functional Materials. *Mol. Phys.* **2018**, *116* (7–8), 1078–1090. https://doi.org/10.1080/00268976.2017.1402966.

(26)   F. Santoro, FCclasses: A Fortran 77 Code; 2008. (Available via the Internet at Http://Www.Pi.Iccom.Cnr.It/Fcclasses; Last Accessed 09/04/2021).

(27)   Shuai, Z.; Peng, Q. Excited States Structure and Processes: Understanding Organic Light-Emitting Diodes at the Molecular Level. *Phys. Rep.* **2014**, *537* (4), 123–156. https://doi.org/10.1016/j.physrep.2013.12.002.

(28)   Lu, T.; Chen, F. Multiwfn: A Multifunctional Wavefunction Analyzer. *J. Comput. Chem.* **2012**, *33* (5), 580–592. https://doi.org/10.1002/jcc.22885.

(29)   Le Bahers, T.; Adamo, C.; Ciofini, I. A Qualitative Index of Spatial Extent in Charge-

Transfer Excitations. *J. Chem. Theory Comput.* **2011**, *7* (8), 2498–2506. https://doi.org/10.1021/ct200308m.

(30) Escudero, D. Quantitative Prediction of Photoluminescence Quantum Yields of Phosphors from First Principles. *Chem. Sci.* **2016**, *7* (2), 1262–1267. https://doi.org/10.1039/c5sc03153b.

(31) Peng, Q.; Yi, Y.; Shuai, Z.; Shao, J. Toward Quantitative Prediction of Molecular Fluorescence Quantum Efficiency: Role of Duschinsky Rotation. *J. Am. Chem. Soc.* **2007**, *129* (30), 9333–9339. https://doi.org/10.1021/ja067946e.

(32) Prlj, A.; Sandoval-Salinas, M. E.; Casanova, D.; Jacquemin, D.; Corminboeuf, C. Low-Lying Ππ* States of Heteroaromatic Molecules: A Challenge for Excited State Methods. *J. Chem. Theory Comput.* **2016**, *12* (6), 2652–2660. https://doi.org/10.1021/acs.jctc.6b00245.

(33) Easterly, C. E.; Christophorou, L. G.; Blaunstein, R. P.; Carter, J. G. Fluorescence from the Second Excited π-Singlet State of 1,2-Benzanthracene and 3,4-Benzopyrene in Solution. *Chem. Phys. Lett.* **1970**, *6* (6), 579–582. https://doi.org/10.1016/0009-2614(70)85231-9.

(34) Geldof, P. A.; Rettschnick, R. P. H.; Hoytink, G. J. Fluorescence from the Second Excited Singlets of Pyrene and 3,4-Benzpyrene. *Chem. Phys. Lett.* **1969**, *4* (2), 59–61. https://doi.org/10.1016/0009-2614(69)85066-9.

(35) Jacquemin, D.; Escudero, D. Thermal Equilibration between Excited States or Solvent Effects: Unveiling the Origins of Anomalous Emissions in Heteroleptic Ru(Ii) Complexes. *Phys. Chem. Chem. Phys.* **2018**. https://doi.org/10.1039/c8cp01101j.

(36) Gupta, V. D.; Tathe, A. B.; Padalkar, V. S.; Umape, P. G.; Sekar, N. Red Emitting Solid

State Fluorescent Triphenylamine Dyes: Synthesis, Photo-Physical Property and DFT Study. *Dye. Pigment.* **2013**, *97* (3), 429–439. https://doi.org/10.1016/j.dyepig.2012.12.024.

(37)   Raikwar, M. M.; Mathew, E.; Varghese, M.; Joe, I. H.; Nethi, S. N. NLOphoric Triphenylamine Derived Donor-π-Acceptor-π-Donor Based Colorants: Synthesis, Spectroscopic, Density Functional Theory and Z-Scan Studies. *Photochem. Photobiol.* **2019**, *95* (4), 931–945. https://doi.org/10.1111/php.13089.

TOC
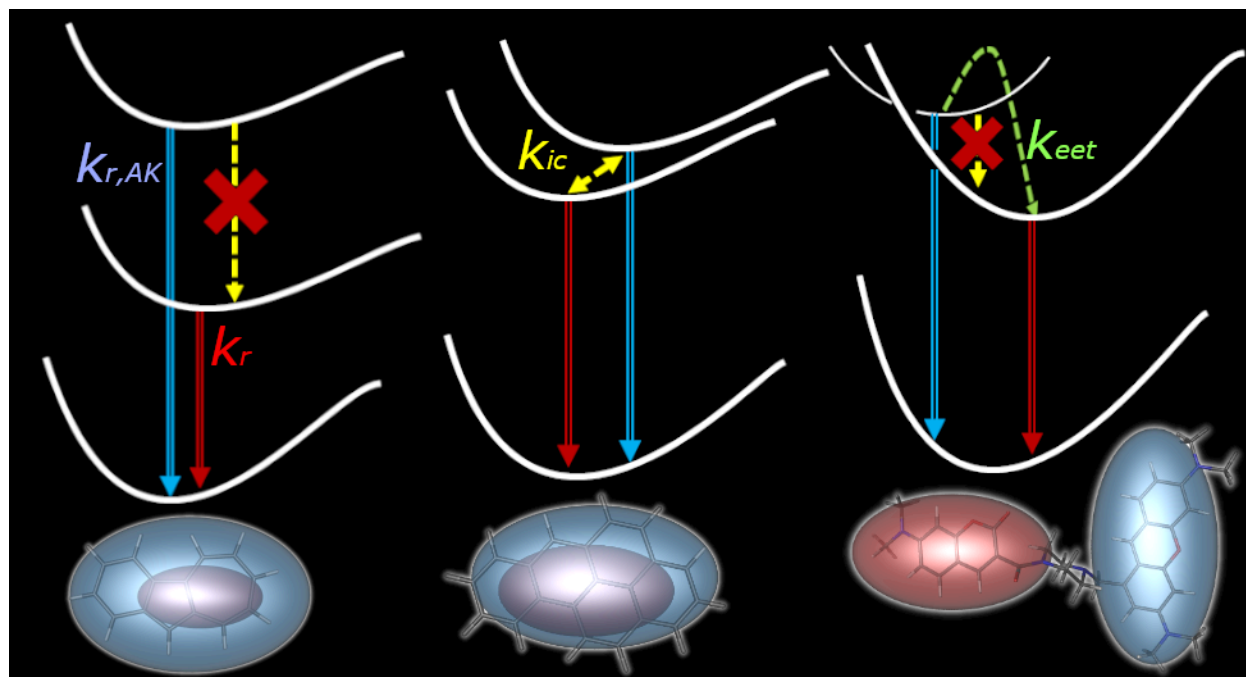
In this Accounts, a classification of different anti-Kasha photoluminescence regimes is provided